



# Countermeasures to treat collapse during the construction of road tunnel in fault zone: a case study from the Yezhuping Tunnel in south Qinling, China

Yaqiong Wang<sup>1</sup> · Hongtao Chang<sup>1</sup> · Jianyu Wang<sup>1,2</sup> · Xiaoli Shi<sup>1</sup> · Junling Qiu<sup>1</sup>

Received: 22 March 2019 / Accepted: 16 July 2019 / Published online: 25 July 2019  
© Springer-Verlag GmbH Germany, part of Springer Nature 2019

## Abstract

To ensure the safety of the tunnel construction, it is very important to take the appropriate treatment measures after the collapse happened. Especially the tunnel goes through the fault fracture zone. This paper sets forth the process of the collapse that occurred in the Yezhuping Tunnel affected by the fault fracture zone and introduces the treatment for the collapse. The deformation characteristics of the surrounding rock are analyzed according to the monitoring results. Based on the research regarding the effect of the fault on the tunnel by using the general Hoek–Brown failure criterion and the field monitoring results, it is shown that the fault is the main reason for the collapse; it induces the attenuation of the Young modulus and the compressive strength and the enlargement of the plastic zone. The research results have some reference significance for similar projects.

**Keywords** Tunnel engineering · Fault zone · Collapse · Treatment · Hoek–Brown (H–B) failure criterion · Field monitoring

## Introduction

As an important part of the expressway in mountainous area, the mountain tunnel plays an increasingly vital role. Many mountain tunnels are constructed in fault fracture zones, as the proper line-type requirements. The rock mass is loose, broken and unstable where it in the fault fracture zone. It is prone to collapse and causes serious casualties and economic losses. Since the surrounding rock is broken and the geological condition of the Yezhuping Tunnel is complicated, the accident caused by construction comes out unexpectedly. Many instability issues in the engineering practice, such as initial support damaged are caused by excessive deformation of the surrounding rock under the influence of fault fracture zone. No matter whether the fault is exposed during excavation, the stability of the tunnel will be affected. According to the monitoring results, nearly 80% of the collapse accidents

are affected by the fault zone in the current underground engineering. We summarize the mountain tunnels that have undergone geological disasters, and find that most of them are built in unfavorable geological areas. Especially when the tunnel goes through the fault fracture zones, it is prone to serious accidents, as shown in Table 1.

Many elaborate researches on this issue had been done. The analysis of physical simulation shows that the magnitudes of rock mass plastic zones will increase with the decreasing of the friction angle of fault (Hao and Azzam 2005). The shear deformation of the tunnel will emerge along the weak plane (Schubert and Riedmüller 1997). It was pointed out that the fault fracture zone leads to significant changes for the structure of the rock mass, through laboratory model tests (Jeon et al. 2004). It was shown that the dip and width of the fault are important factors affecting the stability of surrounding rock by numerical simulation and model test. As the fault fracture zone, the geostress is no longer symmetrical and the different degrees of stress concentration are shown after tunnel excavation (Wang et al. 2017a, b). It was suggested by field experiments that the high geostress and the lithological changes of surrounding rocks caused by the fault are main factors leading to the asymmetric distribution of stress in the deep tunnel (Li et al. 2011). In order to reduce the risk of seismic damage in the

✉ Hongtao Chang  
chang-hongtao@chd.edu.cn

<sup>1</sup> School of Highway, Chang'an University, Xi'an 710064, China

<sup>2</sup> Zhaotong Municipal People's Government Office, Zhaotong 657000, China

**Table 1** Statistics of tunnel accidents caused by fault zone during the construction in China from 2010 to 2017

Tunnel name	Disaster type	Geology of tunnel site	Damage
Baiyun Tunnel	Collapse, water-inrush	Fault fracture zone	6 deaths
Qixiaying Tunnel	Collapse	Influence zone of fault	10 deaths
Xiaopingqiang Tunnel	Collapse	Fault fracture zone	12 deaths
Liulang Tunnel	Collapse of the vault	Fault fracture zone	5 people trapped
Zhipu Tunnel	Face collapse	Influence zone of fault	9 deaths
Manme No. 1 Tunnel	Closure collapse	Fault fracture zone	9 people trapped

fault fracture zone, an articulated lining design was adopted along the active fault zone in Turkey (Russo et al. 2002). The Yanmenguan Tunnel took the method that reserving core soil and using asymmetric lining through the fault (Lin et al. 2017). The Wuzhuling Tunnel took asymmetric lining design and strengthened the thickness of the lining within the fault to overcome stress concentration and uniform stress distribution (Wang et al. 2017a, b). Soil-freezing consolidation was adopted to pass through the Qingquan Street Fault in the Guangzhou Metro Tunnel (Lei et al. 2008). The Guan-jiao Tunnel passed through faults by shortening the time span between the initial support and secondary lining and increasing the amount of shotcrete (Li et al. 2011). Based on researches that information construction and prediction in the tunnel, the tunnel construction is optimized (Zhou et al. 2017). The jet-grouting pile was used to reinforce the soft rock (Wang et al. 2018a, b, c, 2019a, b, c, d, e; Li et al. 2018). Besides, the lithology (Zhang et al. 2018a, b, c; Lai et al. 2018; Yue et al. 2019), groundwater (Wang et al. 2019b; Zhang et al. 2018a, b, c; Zheng et al. 2019), surface subsidence (Wang et al. 2018b, c, 2019a), effect of vibration (Duan et al. 2019a, b; Li et al. 2019a, b), support system (Wang et al. 2017b, 2019b; Zhang et al. 2018a, b, c), concrete characteristics (Wei et al. 2018, 2019) were studied. The effect of the temperature on the rock was discussed (Nie et al. 2018; Wei et al. 2017; Duan et al. 2019a, b).

The above research mainly aims at the surrounding rock control measures to prevent accidents when the tunnel passes through the fault fracture zone, and it has not studied the treatment measures for accidents during the excavation process. In many cases, however, due to the suddenness and concealment of disasters such as tunnel collapse and water-inrush, it is impossible to predict in advance, and the engineering disaster is difficult to avoid (Qiu et al. 2019). Based on the Hoek–Brown failure criterion (Hoek and Brown 1980, 1988, 1997; Marinos and Hoek 2001; Sonmez and Ulusay 1999; Sun and Lu 2008) and the project of the Yezhuping Tunnel, the variation of physical and mechanical properties of surrounding rock of tunnel section affected by the fault fracture zone was analyzed in this paper. The mechanism of the fault on the surrounding rock of the tunnel was discussed, it was concluded that the fault fracture zone is the main cause inducing the collapse of the Yezhuping

Tunnel. The treatment measures for the landslide induced by the fault were introduced, and the results were found to be effective based on the analysis for the on-site monitoring. The results of our research in this paper not only guide in the construction of the Yezhuping Tunnel, but also have certain reference value for similar projects.

## Engineering background

### Project information

The Yezhuping Tunnel is a part of the Dan-Ning Expressway Project (Danyang to Ningshan). As shown in Fig. 1, it is located in Zhashui County, south Qinling, Shangluo City, Shaanxi Province, and it is the connection line between Zhashui and Shanyang. It is a long-separated highway mountain tunnel and about 60 km away from Xi'an. The length of the left line is 2309 m and the right line is 2326 m; the depth of the left line is 523.52 m and the right line is 526.48 m. Figure 2 shows the lithological section of the tunnel. The tunnel is excavated by the bench tunneling method, with a footage of 0.6 m per stage. Generally, the construction of three stages can be completed within 2 days. The Yezhuping Tunnel adopted the lining sections of the three-centered circular arch. The net width of the tunnel is 10.25 m. It is composed by:  $(0.75 + 0.5 + 3.75 \times 2 + 0.75 + 0.75)$  m; a maintaining way was set up in each side of the tunnel. A circular drainage ditch with  $\varphi$  20 cm and a fire pipeline with 60 cm  $\times$  50 cm were set in left maintaining way; a cable duct with 60 cm  $\times$  65 cm was set up in the right. A central drain was set under the roadbed of the tunnel. Figure 3 shows the internal contour design of the tunnel.

### Engineering–geological conditions

The mountain tunnel crossing is a rocky mountain with exposed bedrock and steep terrain. The elevation of the part of the mountain is about 730–1292 m, and the topography undulates greatly. The maximum relative elevation difference is about 562 m. According to the results of the geological mapping and drilling, the rock mass is mainly composed of the slate ( $D_2n$ ) and the quartz schist ( $Z_1$ ), the detritus

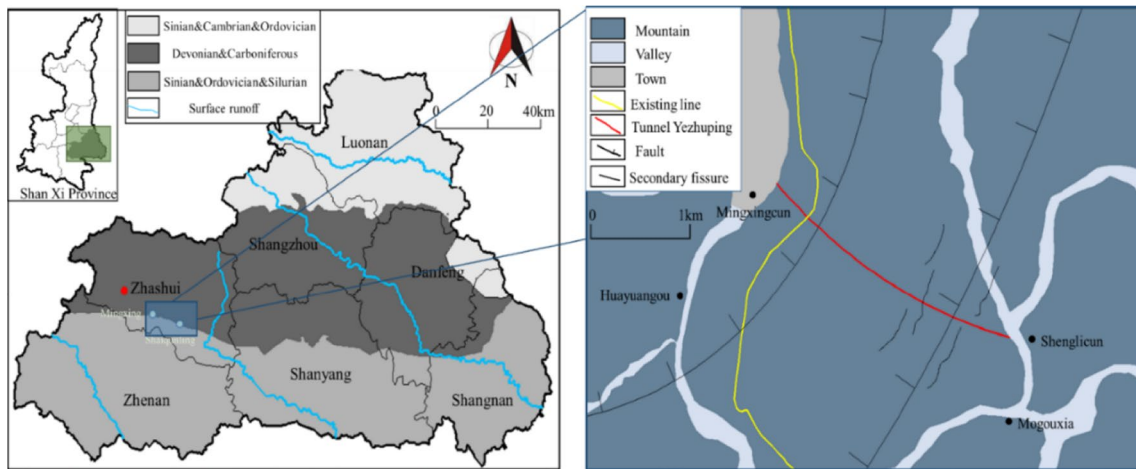


Fig. 1 Location of tunnel

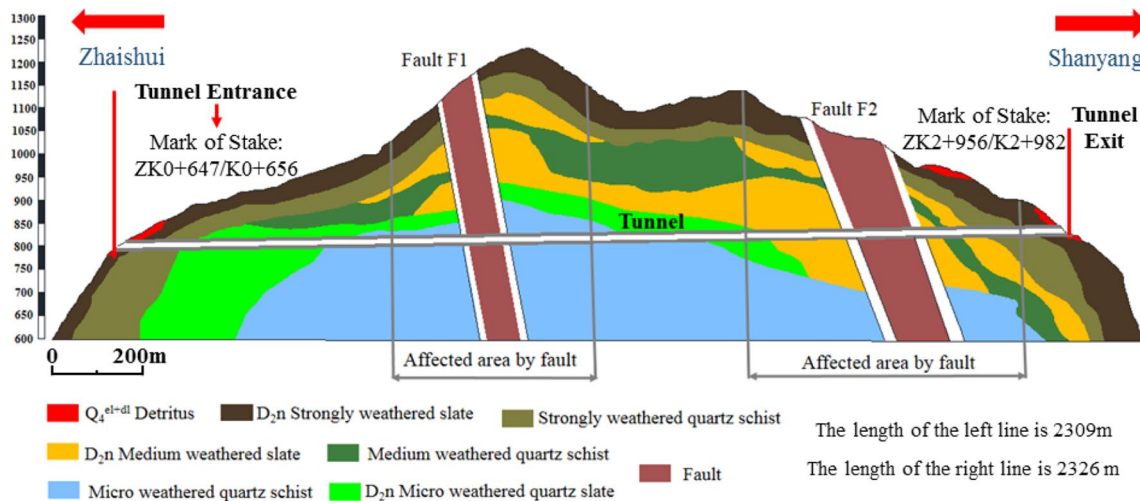


Fig. 2 Longitudinal section of the Yezhuping Tunnel

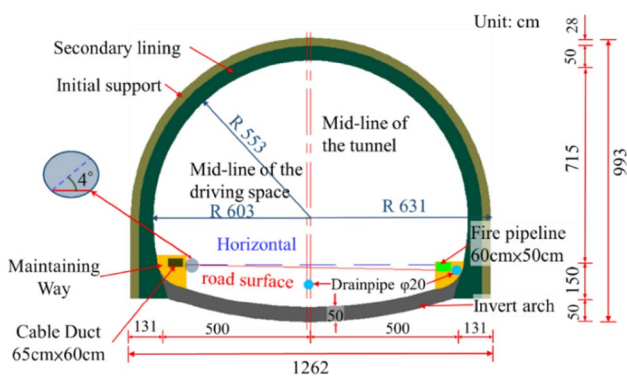


Fig. 3 The internal contour design of the tunnel

( $Q_4^{el+dl}$ ) in the tunnel site. The detritus ( $Q_4^{el+dl}$ ) are mainly composed of gravel soil and rocks and distributed at the entrance and exit of the tunnel. The slate ( $D_{2n}$ ) is one of the main rocks in the tunnel site. It has a palimpsest texture and platy structure. The mineral composition is mainly feldspar and quartz. The joints of rock mass are abundant. It is mainly distributed in the tunnel body. The quartz schist ( $Z_1$ ) is one of the main rocks in the tunnel site. It has a crystalloblastic texture and schistose structure. The mineral composition is mainly chlorite, feldspar and quartz. The joints of the rock mass are abundant. It mainly distributes in the tunnel body.

The landforms of the mountain passed through by the tunnel are precipitous, due to structural erosion and fluvial

incision. The rock (slate and quartz schist) is loose and broken in where the tunnel passed through. According to the measurement during construction, the left line covers 85.25% of the strongly weathered surrounding rock and the right line covers 83.57% of the strongly weathered surrounding rock, as shown in Fig. 2. The groundwater in the tunnel area includes shallow fissure water formed by loose overburden and weathered bedrock and deep cracked water formed by the fault fracture zone. The tunnel passes through two fault fracture zones F1, F2 which contain multiple secondary fracture surfaces.

The F1 Fault, as shown in Fig. 4, is in the Village Yezhuping. The fault surface is inclined to the north; the dip angle is 75°; the width of the fault zone is more than 50 m. The F2 Fault is a north-dipping fault with the dip angle of 79°; there are multiple secondary faults crossing each other. The rock combination is complex, the

maximum thickness between the footwall and hanging wall is about 60 m. The F2 Fault, mainly consisting of three secondary faults which the deformation is concentrated on, is wide in the area around the tunnel exit, but the characteristics of the F2 faults are not obvious.

The section of the Yezhuping Tunnel going through the fault fracture zone with the development of the fracture has a large depth and complex condition of the surrounding rock, the rock mass is broken and unstable which induces collapse easily. According to the research, the fault fracture zone is the main cause leading to the engineering disasters in this project, as shown in Table 2 There are various geological problems in the affected area by the fault fracture zone, such as weak interlayer, the fault gouge, the cavity with the significant scale, and the seriously dripping water, and the rock mass is broken by the core method of sampling, as shown in Fig. 4.

**Fig. 4** Adverse geological phenomena induced by Fault F1

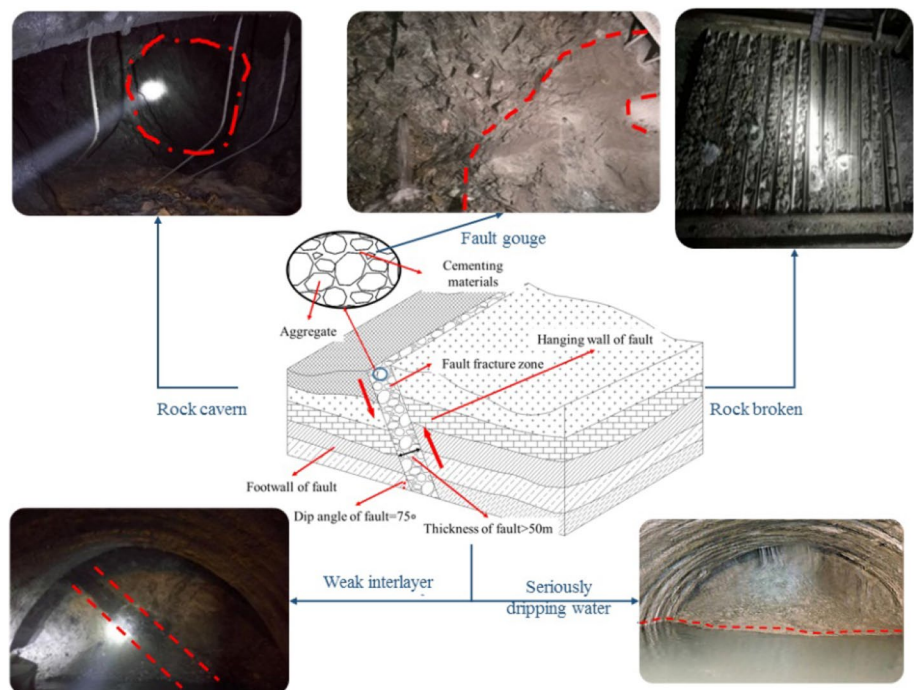


**Table 2** Statistics on large accidents during the tunnel through the fault fracture zone

Date	Accident	Impact on engineering
2017.2.13	Water-inrush and mud-inflow occurred in right line YK2+212	Tunnel face suspended for 40 days Partial passage initial damaged
2017.4.18	Collapse occurred in left line ZK1+410	Partial passage initial damaged
2017.7.3	Collapse occurred in left line ZK1+492	Tunnel face suspended for 20 days Partial passage initial damaged
2017.7.22	Collapse and water-inrush occurred in right line YK1+720	Tunnel face suspended for 20 days Partial passage initial damaged

### Monitoring of the tunnel

During the construction, the deformation of the tunnel has been monitored (Wang et al. 2018, 2019a). Peripheral convergence and vault settlement are the main methods to monitor the dynamic changes of the surrounding rock and confirm the situation of the surrounding rock, and judge the effect of the supporting. The measuring points of the vault settlement were arranged at the vault and each side of the center line 1.5 m away from the center line of the vault. The measuring points of the peripheral convergence were arranged in the same section, as shown in Fig. 5. The location of the monitoring section was determined by the surrounding rock conditions. The monitoring section was arranged for each 20 m with the condition that complete rock mass ( $Q = 1-10$ ),

and arranged for each 10 m with the condition that broken rock mass ( $Q < 1$ ), as shown in Fig. 6. Index  $Q$  is a parameter representing the quality of rock mass in  $Q$  system presented (Barton 1988).  $Q$  is determined by the degree of rock integrity, shear strength of chimera and active stress of surrounding rock. The larger the value, the more complete the rock is. The rank of surrounding rock described by  $Q$  is shown in Table 3.

### The effect of the fault zone

Fault is the main cause of the collapse, so it is necessary to analyze the impact of the faults. The rock failure characteristics are non-linear. Therefore, the Hoek–Brown failure criterion is used to analyze the rock mass of the collapse

Fig. 5 Arrangement of the measuring points and measuring lines in cross section

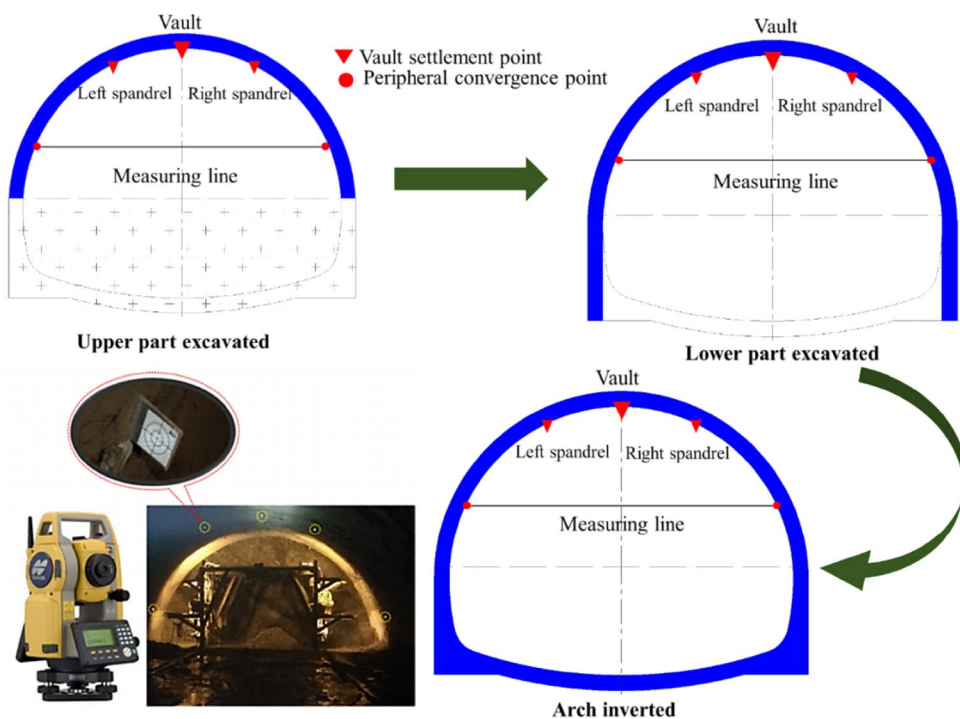
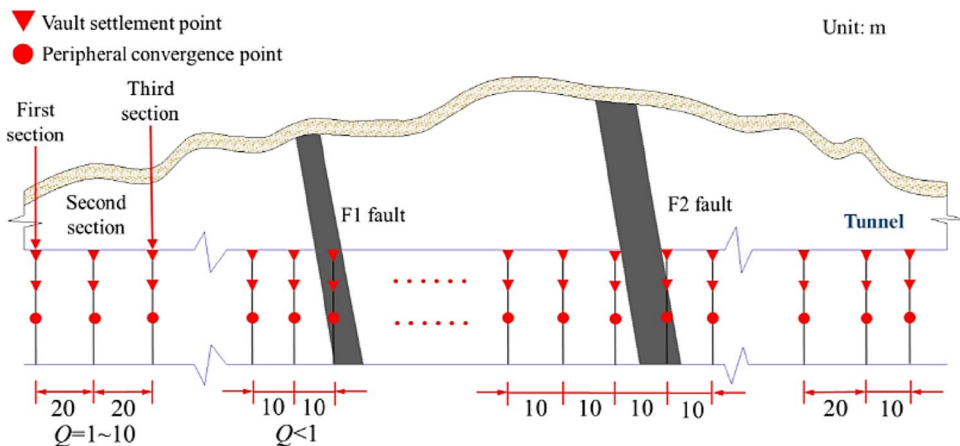


Fig. 6 Arrangement of the monitoring section



**Table 3** Rank of the surrounding rock described by index  $Q$

Value of $Q$	0.001	0.1	1	4	10	40	100	400	1000
Rank	Extremely bad	Rather bad	Bad	Slightly bad	General	Slightly good	Good	Rather good	Extremely good

section. The general Hoek–Brown failure criterion that can be applied to both rock and rock mass was proposed (Hoek and Brown 1988). It can be shown in Eq. 1

$$\sigma_1 = \sigma_3 + \sigma_c \left( m_b \frac{\sigma_3}{\sigma_c} + s \right)^a \tag{1}$$

In the formula:  $\sigma_1$  and  $\sigma_3$  are the maximum and minimum principal stresses.  $\sigma_c$  is the uniaxial compressive strength for rock, the values of  $\sigma_c$  are obtained by the uniaxial compression test. Specifically, we take core sampling drilling, and make rock samples with diameter of 48–52 mm and height–diameter ratio of 2 firstly. Then we conduct the uniaxial compression test with ten specimens per point. The loading rate is 0.5 MPa/s. The average values are taken as the values of  $\sigma_c$ , as shown in Table 4.  $m_b$  and  $a$  are dimensionless empirical parameters of the rock mass.  $s$  is an empirical parameter of the rock mass reflecting the degree of fragmentation of the rock mass. To determine the value of the empirical parameter  $m_b$ ,  $a$ ,  $s$ , a disturbance parameter  $D$  considering stress releasing, and a method for determining the value of parameters was proposed, based on the geological strength index (GSI), as shown in Eq. 2:

$$\left. \begin{aligned} m_b &= \exp \left( \frac{GSI - 100}{28 - 14D} \right) m_i \\ s &= \exp \left( \frac{GSI - 100}{9 - 3D} \right) \\ a &= 0.5 + \frac{1}{6} [\exp(-GSI/15) - \exp(-20/3)] \end{aligned} \right\} \tag{2}$$

In the formula:  $m_i$  is a dimensionless empirical parameter of the rock, reflecting the hardness of the rock. The value of parameter  $m_i$  can be obtained, based on the experience of laboratory and field, as shown in Table 4. The value of GSI can be obtained by interpolating the GSI table (Sonmez and Ulusay 1999).

To study the influence of the fault on different sections of rock mass, the fault model needs to be established firstly. Based on outcrop studies of consolidated rock mass in the fault fracture zone, a fault zone model (Caine and Tomusiak

2003) comprising core zone and surrounding damage zones with different properties and thicknesses was developed. The fault core accommodates most of the strain and displacement of the fault zone and is formed by gouge and cataclasite. The damage zone consists of minor faults and fractures (Aydin and Basu 2005; De Dreuzy et al. 2001; Hestir and Long 1990). The fault model is shown in Fig. 7. In order to reflect intuitively the effect of fault fracture zone on the surrounding rock of the tunnel, three points named A, B, and C are taken along the longitudinal direction of the tunnel in the fault core (close to the collapse section ZK1 + 492) and the fault damage zone and outside the fault zone, as shown in Fig. 7.

In order to obtain empirical parameters of the rock mass characteristics, the value of the disturbance coefficient  $D$  needs to be determined. Abundant engineering practice shows that the loosening and damage of surrounding rock caused by blasting and excavation can be effectively evaluated by measuring and analyzing the propagation velocity of the acoustic wave, and it has good precision. Therefore, it is feasible to evaluate the degree of disturbance of rock mass by measuring the propagation velocity of the acoustic wave (Sun and Lu 2008). In addition, the Young modulus  $E_m$  of the rock mass can be estimated according to the following equations:

$$\left. \begin{aligned} E_m &= \left( 1 - \frac{D}{2} \right) \sqrt{\frac{\sigma_c}{100}} \cdot 10^{[(GSI-10)/40]} \quad (\sigma_c < 100 \text{ MPa}) \\ E_m &= \left( 1 - \frac{D}{2} \right) \cdot 10^{[(GSI-10)/40]} \quad (\sigma_c > 100 \text{ MPa}) \end{aligned} \right\} \tag{3}$$

In the formula: the disturbance parameter of the rock mass is  $D$ , and the average Young modulus is  $E_U$  when the rock mass is not disturbed,  $E_D$  is the average Young modulus of disturbed rock mass. The quotient of  $E_U$  and  $E_D$  obtained by Eq. 3 is:

$$\frac{E_U}{E_D} = \frac{1}{1 - D/2} \tag{4}$$

According to the elastic wave theory, the relationship between the Young modulus of the rock mass and the longitudinal wave propagation velocity can be expressed as:

**Table 4** Partial table for the value of parameter  $m_i$

Rock type	Different texture rocks and their $m_i$ values			
	Rough	Medium	Tiny	Very tiny
Sedimentology	Conglomerate (21 ± 3)	Sandstone (17 ± 4)	Siltstone (7 ± 2)	Shale (6 ± 2)

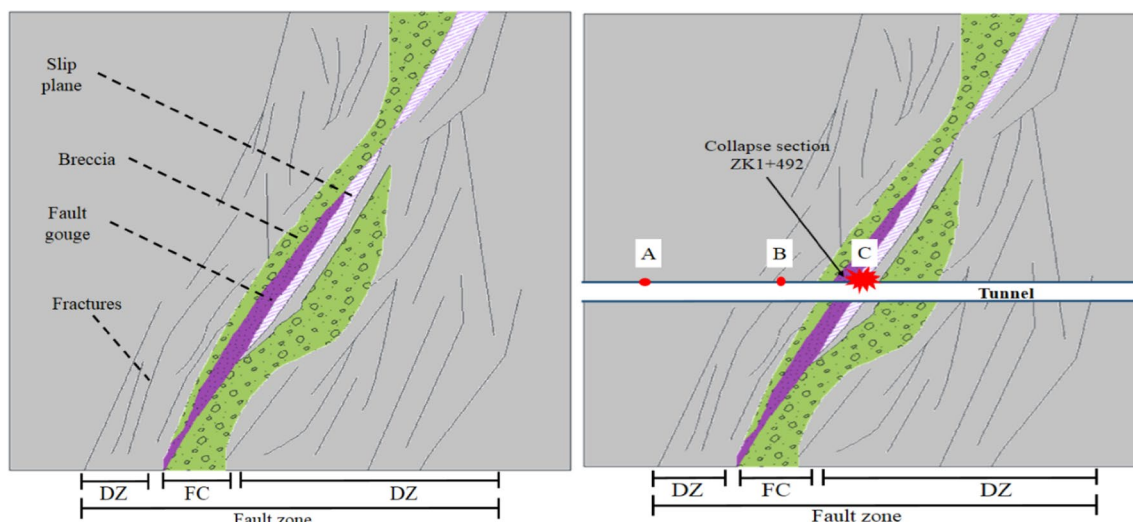


Fig. 7 Fault zone model and position of different stations

$$V_P = \sqrt{\frac{E_m(1 - \mu)}{\rho(1 + \mu)(1 - 2\mu)}} \tag{5}$$

In the formula:  $V_P$  is the longitudinal wave velocity.  $P$  is the density of the rock mass.  $\mu$  is the Poisson ratio. Assume the average longitudinal wave velocity in the undisturbed rock mass be  $V_U$ , the average longitudinal wave velocity in the disturbed rock mass be  $V_D$ . The disturbance parameter  $D$  can be obtained from Eqs. 4, 5, as shown in Eq. 6:

$$D = 2 \left[ 1 - \left( \frac{V_D}{V_U} \right)^2 \right] \tag{6}$$

Although the rock type of points A, B and C is same, due to their different water content and void ratio, the value of  $\sigma_c$  have large differences. According to field and laboratory tests and calculations, the values of the three parameters in points A, B, and C are obtained, as shown in Table 5.

According to the parameters obtained in Eq. 3, the Hoek–Brown criterion for the rock mass corresponding to each measuring point can be established:

$$\left. \begin{aligned} A : \sigma_1 &= \sigma_3 + 1.561 \times (27.696 \cdot \sigma_3 + 3.646)^{0.505} \\ B : \sigma_1 &= \sigma_3 + 0.866 \times (16.431 \cdot \sigma_3 + 0.256)^{0.515} \\ C : \sigma_1 &= \sigma_3 + 0.143 \times (94.017 \cdot \sigma_3 + 0.248)^{0.536} \end{aligned} \right\} \tag{7}$$

Table 5 Parameters of rock mass for each station

Station	Rock type	Location	$m_i$	$\sigma_c$ (MPa)	SI	$V_U$ (m/s)	$V_D$ (m/s)	$D$	$m_b$	$s/10^{-4}$	$a$
A	Slate	Outside of FZ	9	51.09	2	2423	2330	0.15	1.415	36.464	0.505
B	Slate	DZ	9	30.37	36	1338	1189	0.42	0.499	2.564	0.515
C	Slate	FZ	9	19.89	23	1008	849	0.58	0.187	0.248	0.536

In order to get intuitive analysis results, linear regression analysis to Eq. 7, and the equivalent Mohr–Coulomb failure criterion formula are shown in Eq. 8:

$$\sigma_1 = \frac{1 + \sin \varphi}{1 - \sin \varphi} \sigma_3 + \frac{2c \cos \varphi}{1 - \sin \varphi} \tag{8}$$

In order to ensure the fitness of the parameters, the range of the minimum principal stress is  $\sigma_3 \in (0, 0.5\sigma_c)$ . The equivalent M–C failure criterion formula is available:

$$A : \sigma_1 = 2.343267\sigma_3 + 11.510433, \tag{9}$$

$$B : \sigma_1 = 1.805349\sigma_3 + 3.682924, \tag{10}$$

$$C : \sigma_1 = 1.476631\sigma_3 + 1.258120. \tag{11}$$

The parameters of the physical and mechanical properties of the rock mass including Young modulus  $E_m$ , cohesive force  $c$ , internal friction angle  $\varphi$ , compressive strength  $\sigma_{cn}$ , were solved by using Eqs. 3, 8–11. The results are shown in Table 6.

From the data of Table 6, some conclusions can be drawn.

- (1) Compared to the parameters of rock mass outside the fault, the Young modulus of the rock mass in the damage zone has decreased by 73.78%, the cohesion has decreased by 63.54%, the inner friction angle has

**Table 6** Parameters of physical and mechanical properties for each station

Station	$E_m$ (MPa)	$C$ (MPa)	$\Phi$ (°)	$\sigma_{cn}$ (MPa)
A	7.418	3.760	23.9	11.510
B	1.945	1.371	16.9	3.683
C	0.669	0.518	11.1	1.258

decreased by 29.28%, and the compressive strength has decreased by 68.00%.

- (2) Compared to the parameters of rock mass outside the fault, the Young modulus of the rock mass in the fault core has decreased by 90.98%, the cohesion has decreased by 86.22%, the inner friction angle has decreased by 53.56%, and the compressive strength has decreased by 89.07%.
- (3) Compared to the parameters of rock mass in the fault damage zone, the Young modulus of the rock mass in the fault core has decreased by 65.60%, the cohesion has decreased by 62.22%, the inner friction angle has decreased by 34.32%, and the compressive strength has decreased by 65.84%.

It can be shown that the shorter distance between the tunnel face and the fault core, the smaller Young modulus, cohesion, internal friction angle and compressive strength. The shear strength of the surrounding rock gradually decreases, and the plastic zone becomes increasingly large, the load capacity of the surrounding rock is gradually smaller.

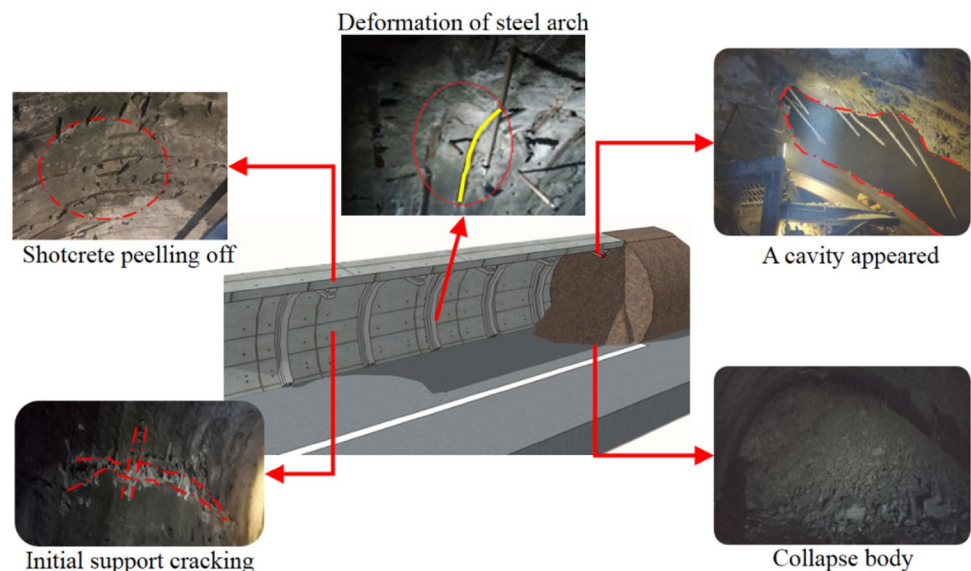
## Collapse and treatment

### Overview of the collapse

In July 2017, the vault rock dropped and the water emerged by seepage in the tunnel face of the section ZK1 + 492 in the left line of the tunnel. Then the collapse happened in the position of the vault after closing the tunnel face. The collapse spread from the left side to the right side along the arch ring. The slag body slid off from the vault intermittently, and the collapse body mainly composed of loose mixture of soil and rock, and most of the rock was fully weathered mudstone with the black mud. The collapse length was estimated to be no less than 5 m, the volume of the collapse body was roughly estimated to be about 110 m<sup>3</sup>, as shown in Fig. 8. The collapse also had a serious impact on the excavated section. The initial support was damaged such as deformation of the steel arch, cracking and spalling of the shotcrete layer by this collapse, as shown in Fig. 8.

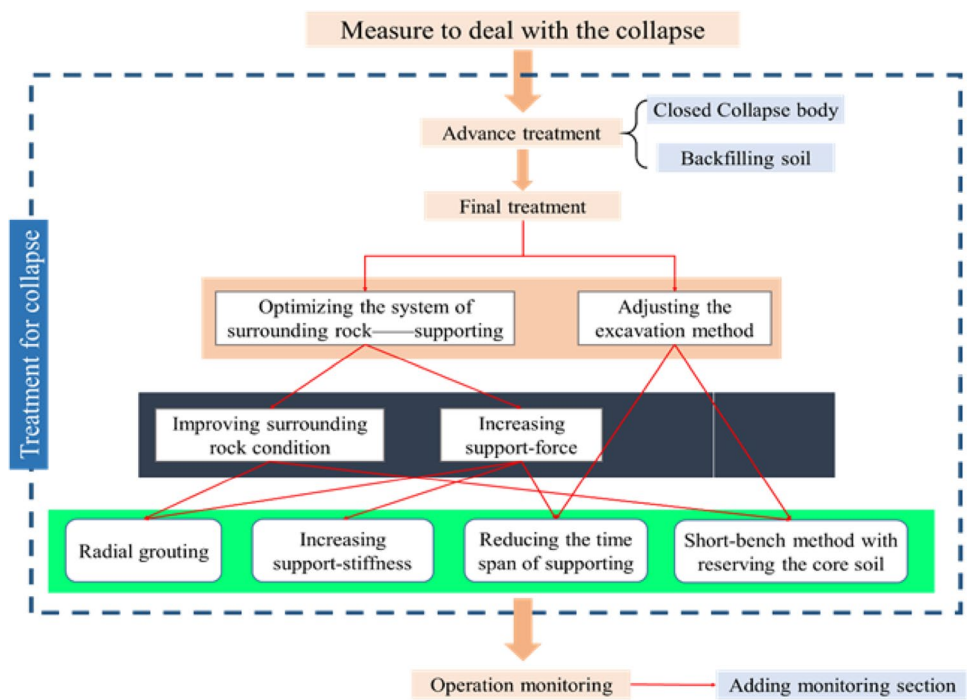
### Treatment for collapse

In order to avoid secondary disasters happened, the emergency measures that stopping excavation, closing the collapse body, and backfilling the back-pressure soil were taken immediately. The treatment measures for this collapse were started from two aspects, on the one hand, improving the bearing capacity of the surrounding rock-support system, the key is to enhance the surrounding rock conditions of the tunnel, and improve the bearing capacity of the support. On the other hand, adjusting the excavation method and strengthening the monitoring. The treatment measures are shown in Fig. 9.

**Fig. 8** Collapse field of section ZK1 + 492



**Fig. 9** The scheme for treatment of collapse



**Advance treatment**

Stopping the excavation and treating the collapse body firstly after the collapse occurred. The collapse body was sealed by spraying C20 concrete and steel mesh to form an overall force body, so that it can be uniformly stressed. The gravel and soil are transported from outside the tunnel, and they are used as back-pressure soil, then they are backfilled on the tunnel face. They provide back pressure and prevent the occurrence of secondary collapse. There are two layers of back-pressure soil. The first layer adopts manual compaction to avoid disturbance, the thickness is 50 cm. The second layer is mechanically compacted, and the thickness of the second layer is 3 m. The back-pressure soil had a length of 5 m and the area accounted for two-thirds of the tunnel face, as shown in Fig. 10.

**Radial grouting**

In order to improve the integrity of the surrounding rock, and reduce the damage to the surrounding rock by the fault fractured zone, the radial grouting was adopted which was also the main measure to plug water. The specific technique is: adjust the systematic rock bolt (mortar rock bolt) to  $\varnothing 50 \times 4$  mm grouting pipe (5 m length, 120 cm longitudinal spacing, 25 per ring). To ensure slurry can quickly condense under dynamic water conditions, this measure adopts the cement–sodium silicate binary slurry. The cement–sodium silicate binary slurry application was applied in which  $120^\circ$  of the arch part. The ordinary cement slurry was applied in other part. The grouting sequence was from top to bottom and from the vault to the sides, as shown in Fig. 11. The specific slurry is shown in Table 7.

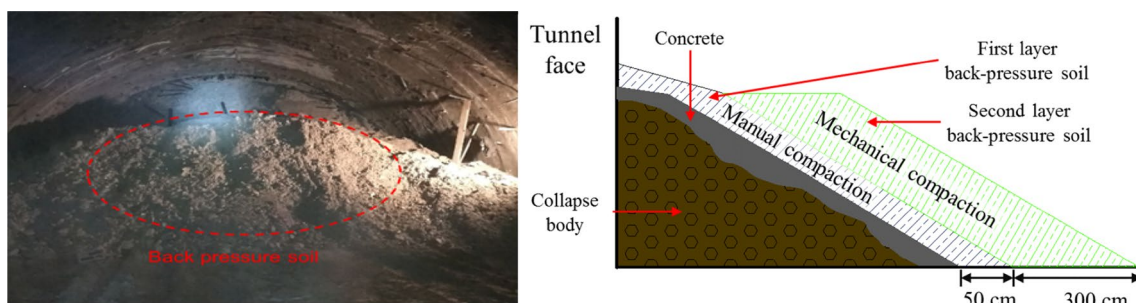


**Fig. 10** Backfilling of field back-pressure soil and vertical sketch of the back-pressure soil

**Fig. 11** Schematic diagram of radial grouting and supporting

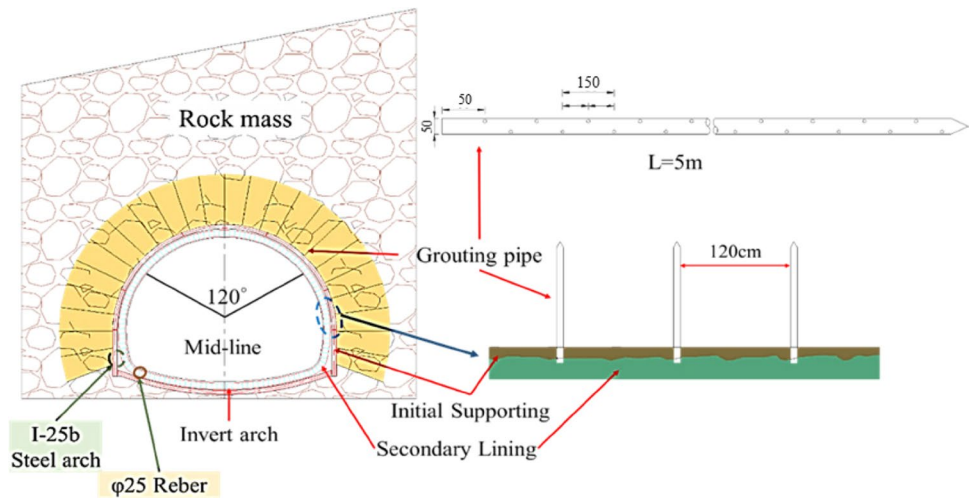


**Table 7** Slurry ratio parameter table

No.	Type	Proportional parameters			
		Water–cement ratio (W/C)	Volume ratio	Concentration of water–glass (kg/m <sup>3</sup> )	Initial pressure/ final pressure (MPa)
1	Ordinary cement slurry single-shot grouting	W:C = (0.8–1): 1	–	–	0.4–0.8/1.0–1.2
2	Ordinary concrete–water glass two-shot grouting	W:C = (0.8–1): 1	C:S = 1:1	1320	0.4–1.2/1.8–3

**Table 8** Adjustment for parameter of support structure

Succession	Support structure	Before the collapse		After the collapse	
		Model	Distance	Model	Distance
Initial supporting	Steel arch shelf	I22a	80 cm	I25b	60 cm
Secondary lining	Rebar	–		Adding φ 25 rebar	

**Increasing support-stiffness**

It is necessary to improve the bearing capacity of the supporting to ensure the safety of construction while improving the physical and mechanical properties of surrounding rock (Li et al. 2019a, b). The parameters of the supporting in the collapse section were adjusted to improve the stiffness of the supporting. The specific measures are as follows: adjusting the type of the steel arch shelf from I22a to I25b with 60 cm spacing, the secondary lining added φ 25 rebar as shown in Table 8.

**Adjustment of excavation method**

The bench method was used to excavate in the collapse section before the collapse occurred. In order to avoid the

disasters such as collapse happened again, the excavation method was adjusted. Compared with the original method, the new methods include two aspects, on the one hand, the spacing between the upper and lower bench was reduced from; on the other hand, reserving the core soil, as shown in Fig. 12. The slope of core soil is 5:1, and the height of the upper core soil is 3 m, the height of lower core soil is 4 m. The other parameters of the new method are shown in Fig. 13. Although this method extends the construction period, it is conducive to the stability of the tunnel face.

In addition, these measures were taken that reducing the time interval between processes and adjusting the sequence of each process, building the inverted arch in time, and the initial support closely followed the tunnel face to ensure the safety under construction.

**Fig. 12** Core soil and its mechanism

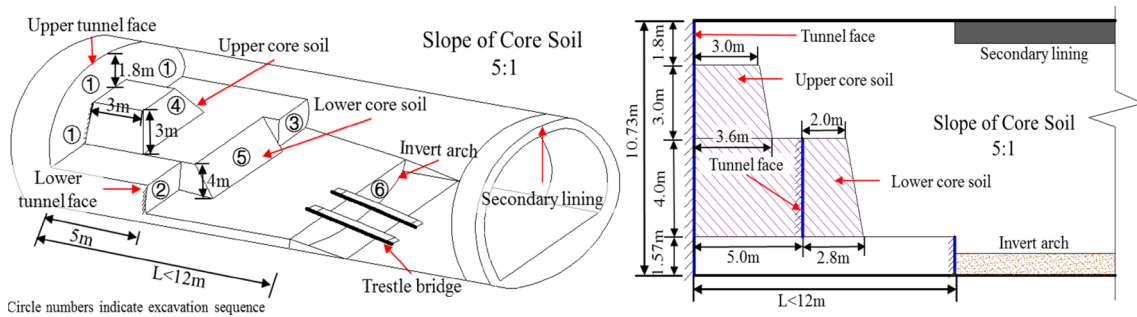
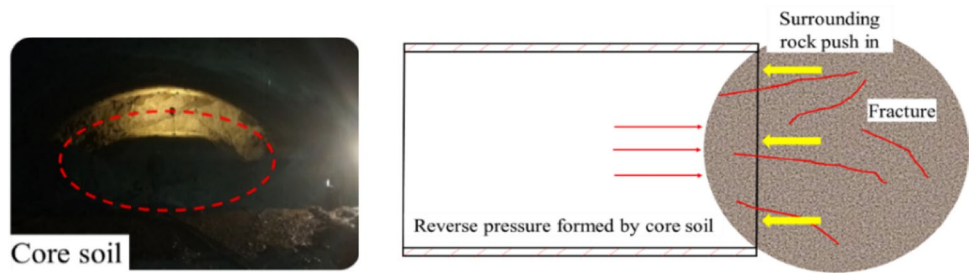
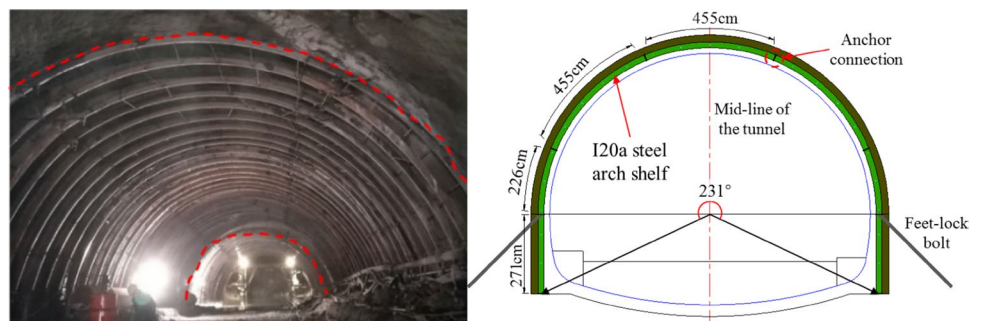


**Fig. 13** Sketch of the new excavation method

**Fig. 14** Spalling and cracking of concrete in the affected section



**Fig. 15** Temporary reinforcement was used in the affected section



**Measure for the affected section**

The supported sections within 30 m behind the collapse were affected after collapse occurred. The phenomenon of spalling and cracking of concrete appeared in the initial support of these sections, as shown in Fig. 14. Therefore,

the I20a steel arch shelf is used for circumferential reinforcement in the affected section (Wang et al. 2017a, b). The range of the temporary reinforcement section is 30 m. The steel arch frame is fixed and connected by anchor, as shown in Fig. 15. The parameters of temporary reinforcement are shown in Table 9.

**Table 9** Parameters of temporary reinforcement

Range of reinforcement	Method	Material	Range of angle for a ring	Distance between rings	Connection type
30 m	Circumferential reinforcement	I20a steel arch shelf	231°	30 cm	Anchor

## Analysis and discussion

### Deformation characteristics of surrounding rock

Many engineering disasters occurred in the Yezhuping Tunnel were concentrated in the fault fracture zone, so it is necessary to strengthen the monitoring on the fault fracture zone. In addition, the other section of the tunnel was impacted by this collapse, such as the section ZK1 + 480 and ZK1 + 589 as shown in Fig. 16. Based on the monitoring data before taking the treatment, some deformation regularities of the surrounding rock in the affected section could be obtained. Figures 17 and 18 show the monitoring data of the section ZK1 + 480 and ZK1 + 589 separately.

According to the data in Figs. 17 and 18, the deformation regularities of the surrounding rock in the fault fracture zone could be obtained as follows:

- (1) *Large amount of deformation* The significant plastic deformation occurred in surrounding rock of the fault fracture zone. For example, the maximum vault settlement of the section ZK1 + 480 reached 235.8 mm, and the section ZK1 + 589 is 365.5 mm.
- (2) *Fast deformation rate* The deformation rate of the surrounding rock in the fault fracture zone is very large after excavation. The deformation rate was susceptible to the disturbance. For example, the deformation rate of the section ZK1 + 480 suddenly increased after the collapse occurred.
- (3) *Long deformation time* The surrounding rock of the fault section that tunnel passes through continued to

deform for a long time after excavation. It had obvious creep deformation characteristics.

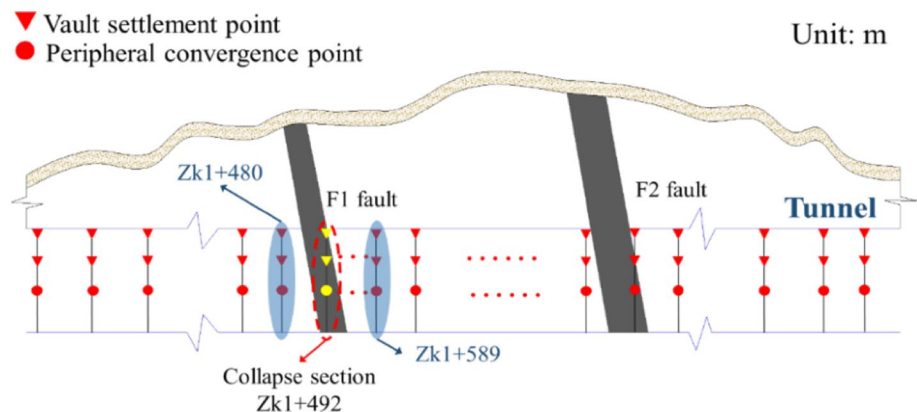
- (4) *Uncoordinated deformation* The uncoordinated deformation of the surrounding rock in the fault fracture zone showed the large difference between different positions of the same section. For example, the cumulative settlement of the right spandrel of the section ZK1 + 589 was 3.6 times than the left spandrel and 3.7 times than the vault.

### Treatment effect

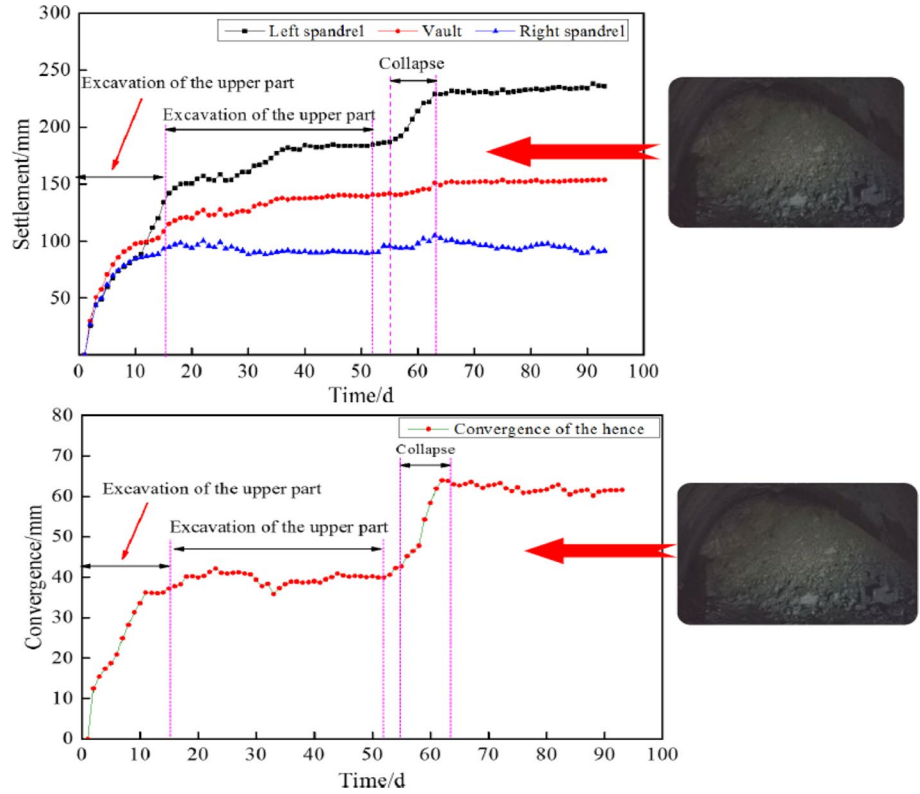
The tunnel was excavated by the Bench Method with reserving core soil after the treatment was completed. We strengthened the monitoring for the initial support of the section where the collapse occurred (ZK1 + 492), after the re-excavation. Monitoring data of the section ZK1 + 492 was obtained, and was compared with that of the section ZK1 + 480. The monitoring data of the section ZK1 + 492 are shown in Fig. 19:

It was concluded from Figs. 17 and 19 that the maximum cumulative value of the vault settlement of the section ZK1 + 492 was 134 mm, and the cumulative value of the peripheral convergence was 148 mm. The deformation trend of the surrounding rock in the section ZK1 + 492 was the same as that in the section ZK1 + 480. The monitoring data showed that as the disturbance of excavation for the lower step, the value of the left spandrel settlement in the section ZK1 + 492 increased. But the increment is obviously lower than that in the section ZK1 + 480. The deformation of the surrounding rock was stabilized in the short term. Phenomena such as the

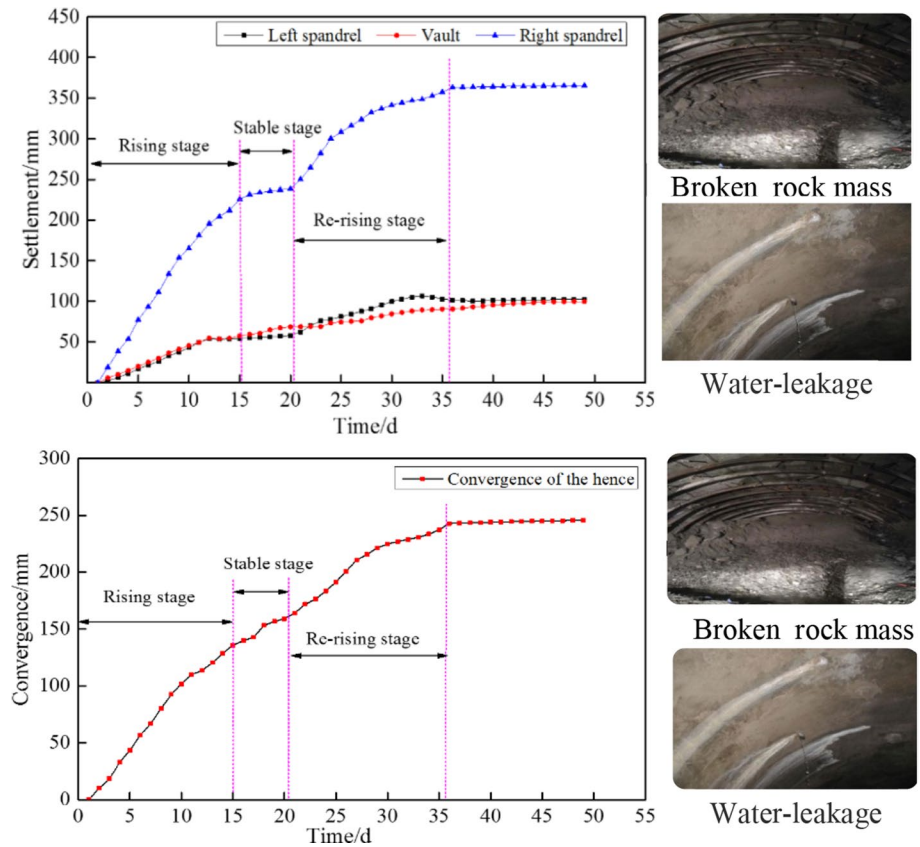
**Fig. 16** Location of representative monitoring section



**Fig. 17** The vault settlement and surrounding convergence datagram of the section ZK1 + 480



**Fig. 18** The vault settlement and surrounding convergence datagram of the section ZK1 + 589



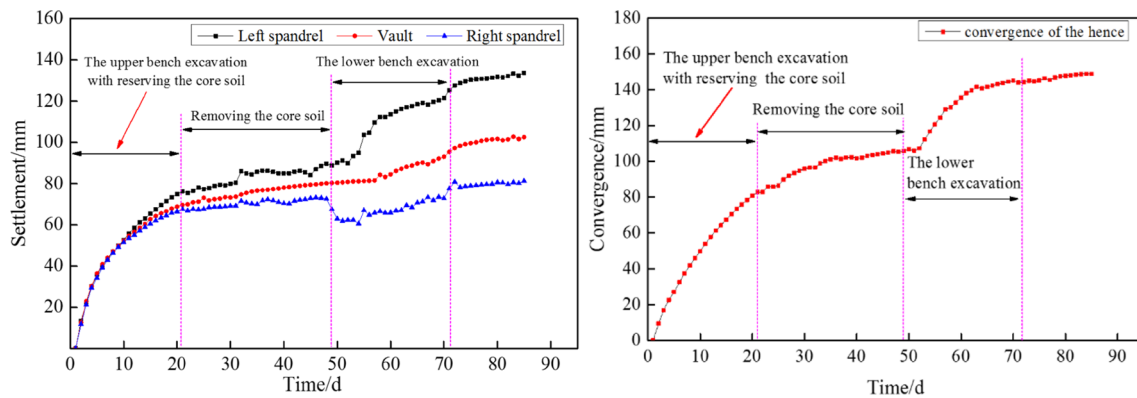


**Fig. 19** The vault settlement and surrounding convergence datagram of collapse section ZK1 + 492

abnormal deformation of the initial support and the cracking of the initial support during the monitoring period did not occur. The treatment proved to be effective.

## Conclusion

In this paper, a case study involving tunnel through the fault zone in the south Qingling mountain region in China was provided and studied in terms of the geological survey, namely extreme deformation characteristics and collapse induced by the fault, effective countermeasures. The effectiveness and rationality of the countermeasures were verified based on the on-site tunnel monitoring (Lai et al. 2018). The geotechnical engineering properties of the impact of the fault on the tunnel were discussed and studied. The valid countermeasures of this case can provide a meaningful reference to similar projects. Based on the findings of this study, the following conclusions can be drawn:

Fault fracture zone is the main factor inducing the collapse. It causes the surrounding rock with broken and well-developed joints which is challenging to construct tunnels. According to the Hoek–Brown failure criterion, the compressive strength and shear strength of the surrounding rock were significantly reduced. Specifically, in the damage zone, the Young's modulus has decreased by 73.78%, the cohesion has decreased by 63.54%, the inner friction angle has decreased by 29.28%, the compressive strength has decreased by 68.00%; In the fault core, the Young's modulus has decreased by 90.98%, the cohesion has decreased by 86.22%, the inner friction angle has decreased by 53.56%, the compressive strength has decreased by 89.07%. The deformation characteristics of the surrounding rock in the collapse section of the Yezhuping Tunnel are controlled by the fault fracture zone. The main features are: (1) fast deformation rate; (2) large amount of deformation; (3) long deformation time; (4) poor stability; (5) uncoordinated deformation.

The proposed countermeasures mainly include the following: (1) backfilling the back-pressure soil backfill; (2) radial grouting; (3) increasing support-stiffness; (4) adjusting excavation method to two-bench reserving core soil method; (5) strengthen stability of the section affected by the collapse with Steel Arch Shelf. According to the monitoring results after treatment, the amount of maximum deformation in the rock mass significantly decreased. Specifically, the maximum vault subsidence and horizontal convergence were 13.8 cm and 15.3 cm, the maximum vault settlement was approximately 2/3 of the values in the section ZK1 + 480 before treatment. The achievement confirmed that these measures can markedly decrease the displacement amount and the effectiveness of the proposed countermeasures.

**Acknowledgements** The research based on the study was funded by the National Natural Science Foundation of China (NSFC) (Grant no. 41702287), the Fundamental Research Funds for the Central Universities (Grant no. 300102218517) and the National Key R&D Program of China (Grant no. 2017YFC0805300) and the Science and Technology Plan in Shanxi Province of China (Grant no. S2018-YF-YBSF-0069). These financial supports are gratefully acknowledged. The authors are grateful to the support to the researchers for their assistance for the study.

**Data availability** The data used to support the findings of this study are available from the corresponding author upon request.

## Compliance with ethical standards

**Conflict of interest** The authors declare that they have no conflicts of interest.

## References

- Aydin A, Basu A (2005) The Schmidt hammer in rock material characterization. *Eng Geol* 81(1):1–14

- Barton NR (1988) Rock mass classification and tunnel reinforcement selection using the Q-system. *Rock Classif Syst Eng Purposes ASTM Int.* <https://doi.org/10.1520/STP48464S>
- Caine JS, Tomusiak SRA (2003) Brittle structures and their role in controlling porosity and permeability in a complex Precambrian crystalline-rock aquifer system in the Colorado Rocky Mountain Front Range. *Geol Soc Am Bull* 115(11):1410–1424
- De Druzy JR, Davy P, Bour O (2001) Hydraulic properties of two-dimensional random fracture networks following a power law length distribution: 1. Effective connectivity. *Water Resour Res* 37(8):2065–2078
- Duan LM, Lin WS, Lai JX, Zhang P, Luo YB (2019a) Vibration characteristic of high-voltage tower influenced by adjacent tunnel blasting construction. *Shock Vib.* <https://doi.org/10.1155/2019/8520564>
- Duan LM, Zhang YH, Lai JX (2019b) Influence of ground temperature on shotcrete-to-rock adhesion in tunnels. *Adv Mater Sci Eng.* <https://doi.org/10.1155/2019/8709087>
- Hao YH, Azzam R (2005) The plastic zones and displacements around underground openings in rock masses containing a fault. *Tunn Undergr Space Technol* 20(1):49–61
- Hestir K, Long JCS (1990) Analytical expressions for the permeability of random two-dimensional Poisson fracture networks based on regular lattice percolation and equivalent media theories. *J Geophys Res Solid Earth* 95(B13):21565–21581
- Hoek E, Brown ET (1980) Empirical strength criterion for rock masses. *J Geotech Geoenviron Eng* 106(ASCE15715):1013–1035
- Hoek E, Brown ET (1988) The Hoek–Brown failure criterion—a 1988 update. *J Heuristics* 16(2):167–188
- Hoek E, Brown ET (1997) Practical estimates of rock mass strength. *Int J Rock Mech Min Sci* 34(8):1165–1186
- Jeon S, Kim J, Seo Y, Hong C (2004) Effect of a fault and weak plane on the stability of a tunnel in rock—a scaled model test and numerical analysis. *Int J Rock Mech Min Sci* 41:658–663
- Lai JX, Wang XL, Qiu JL, Chen JX, Hu Z, Wang H (2018) Extreme deformation characteristics and countermeasures for a tunnel in difficult grounds in southern Shaanxi, China. *Environ Earth Sci* 77(19):1–14
- Lei J, Bai M, Xu Z, Zhang A, Huo Y, Wang P (2008) In-situ test on construction effect with freezing method for fault-crossing fragmentation zone in metro tunnel. *Chin J Rock Mechan Eng* 27(7):1492–1498 (In Chinese)
- Li D, Fu LZ, Sheng LY (2011) Research on the mechanical characteristics of primary supports in Guanjiào tunnel fault fracture zone and its influence zone by field tests. *Appl Mech Mater* 105:1203–1210
- Li Y, Xu S, Liu H, Ma E, Wang L (2018) Displacement and stress characteristics of tunnel foundation in collapsible loess ground reinforced by jet grouting columns. *Adv Civil Eng.* <https://doi.org/10.1155/2018/2352174>
- Li YY, Lin WS, Zhang YW, Wang K (2019) Vibration characteristics and damage repair of the railway tunnel base. *Adv Civil Eng* 16 (Article ID: 1097203)
- Li PF, Wang F, Fan LF, Wang HD, Ma GW (2019b) Analytical scrutiny of loosening pressure on deep twin-tunnels in rock formations. *Tunn Undergr Space Technol* 83:373–380
- Lin D, Yuan R, Shang Y, Bao W, Wang K, Zhang Z, Li K, He W (2017) Deformation and failure of a tunnel in the restraining bend of a strike–slip fault zone: an example from Hengshan Mountain, Shanxi Province, China. *Bull Eng Geol Environ* 76(1):263–274
- Marinos P, Hoek E (2001) Estimating the geotechnical properties of heterogeneous rock masses such as flysch. *Bull Eng Geol Environ* 60(2):85–92
- Nie X, Wei X, Li X, Lu C (2018) Heat treatment and ventilation optimization in a deep mine. *Adv Civil Eng.* <https://doi.org/10.1155/2018/1529490>
- Qiu JL, Qin YW, Feng ZH, Wang LX, Wang K (2019) Safety risks and protection measures for the city wall during the construction and operation of Xi'an Metro. *J Perform Constr Facilities* 1:1. [https://doi.org/10.1061/\(ASCE\)CF.1943-5509.0001342](https://doi.org/10.1061/(ASCE)CF.1943-5509.0001342)
- Russo M, Germani G, Amberg W (2002) Design and construction of large tunnel through active faults: a recent application. In: Proceedings of the International Conference of “Tunnelling and Underground Space Use” (Istanbul, Turkey, 16–18 October 2002), pp 16–18
- Schubert W, Riedmüller G (1997) Influence of faults on tunneling. *Felsbau* 15(6):483–488
- Sonmez H, Ulusay R (1999) Modifications to the geological strength index (GSI) and their applicability to stability of slopes. *Int J Rock Mech Min Sci* 36(6):743–760
- Sun JS, Lu WB (2008) Modification of Hoek–Brown criterion and its application. *Eng J Wuhan Univ* 41(1):63–65 (In Chinese)
- Wang Y, Jing H, Su H, Xie J (2017a) Effect of a fault fracture zone on the stability of tunnel-surrounding rock. *Int J Geomech.* [https://doi.org/10.1061/\(ASCE\)GM.1943-5622.0000837](https://doi.org/10.1061/(ASCE)GM.1943-5622.0000837)
- Wang YQ, Xin YX, Xie YL, Li J, Wang Z (2017b) Investigation of mechanical performance of prestressed steel arch in tunnel. *Front Struct Civ Eng* 11(3):360–367
- Wang ZF, Cheng WC, Wang YQ (2018a) Investigation into geohazards during urbanization process of Xi'an, China. *Nat Hazards* 92(3):1937–1953
- Wang YQ, Kong WK, Wang ZF (2018b) Effect of expanding a rectangular tunnel on adjacent structures. *Adv Civ Eng.* <https://doi.org/10.1155/2018/1729041>
- Wang ZF, Shen JS, Cheng WC (2018c) Simple method to predict ground displacements caused by installing horizontal jet-grouting columns. *Math Problems Eng.* <https://doi.org/10.1155/2018/1897394>
- Wang Z, Hu Z, Lai J, Wang H (2019a) Settlement characteristics of jacked box tunneling underneath a highway embankment. *J Perform Constr Facilities.* [https://doi.org/10.1061/\(ASCE\)CF.1943-5509.0001269](https://doi.org/10.1061/(ASCE)CF.1943-5509.0001269)
- Wang XL, Lai JX, Garnes R, Luo YB (2019b) On the support system for tunnelling in squeezing ground of Qingling-Daba mountainous area: case study from soft rock tunnels. *Adv Civ Eng* 1:1. <https://doi.org/10.1155/2019/8682535>
- Wang ZF, Shen SL, Modoni G (2019c) Enhancing discharge of spoil to mitigate disturbance induced by horizontal jet grouting in clayey soil: theoretical model and application. *Comput Geotech* 111:222–228
- Wang YQ, Xu SS, Ren R, Zhang SZ, Ren ZD (2019d) Application of the twin-tube complementary ventilation system in large-slopping road tunnels in China. *Int J Ventilation.* <https://doi.org/10.1080/14733315.2018.1549305>
- Wang YQ, Wang ZF, Cheng WC (2019e) A review on land subsidence caused by groundwater withdrawal in Xi'an, China. *Bull Eng Geol Environ* 78(4):2851–2863
- Wei Y, Liang S, Guo W, Hansen W (2017) Stress prediction in very early-age concrete subject to restraint under varying temperature histories. *Cement Concr Compos* 83:45–56
- Wei Y, Gao X, Liang S (2018) A combined SPM/NI/EDS method to quantify properties of inner and outer C–S–H in OPC and slag-blended cement pastes. *Cement Concr Compos* 85:56–66
- Wei Y, Gao X, Wang F, Zhong Y (2019) Nonlinear strain distribution in a field-instrumented concrete pavement slab in response to environmental effects. *Road Mater Pavement Design* 20(2):367–380
- Yue XB, Xie YL, Zhang HG, Niu YP (2019) Study on geotechnical characteristics of marine soil at Hongkong–Zhuhai–Macao tunnel. *Mar Georesour Geotechnol.* <https://doi.org/10.1080/1064119X.2019.1609632>
- Zhang Z, Shi X, Wang B, Li H (2018a) Stability of NATM tunnel faces in soft surrounding rocks. *Comput Geotech* 96:90–102

- Zhang N, Shuilong Shen J, Zhou A, Arulrajah A (2018b) Tunneling induced geohazards in mylonitic rock faults with rich groundwater: a case study in Guangzhou. *Tunn Undergr Space Technol* 74:262–272
- Zhang HJ, Wang ZZ, Lu F, Xu GY, Qiu WJ (2018c) Analysis of the displacement increment induced by removing temporary linings and corresponding countermeasures. *Tunn Undergr Space Technol* 73:236–243
- Zheng YC, Xiong J, Liu T, Yue XB, Qiu JL (2019) Performance of a deep excavation in Lanzhou Strong Permeable Sandy Gravel Strata. *Arab J Geosci* 12(16):12
- Zhou W, Qin H, Qiu J, Fan H, Lai J, Wang K, Wang L (2017) Building information modelling review with potential applications in tunnel engineering of China. *Royal Soc Open Sci* 4(8):170–174

**Publisher's Note** Springer Nature remains neutral with regard to jurisdictional claims in published maps and institutional affiliations.